Journal of Molecular Catalysis A: Chemical 316 (2010) 163–170

Contents lists available at ScienceDirect

Journal of Molecular Catalysis A: Chemical

journal homepage: www.elsevier.com/locate/molcata

Visible light photocatalytic degradation of nitric oxides on PtO_x-modified TiO_2 via sol–gel and impregnation method

Chun-Hung Huang[a], I-Kai Wang[a,*], Yu-Ming Lin[b,**], Yao-Hsuan Tseng[c], Chun-Mei Lu[d]

[a] Department of Chemical Engineering, National Tsing-Hua University, Hsinchu 30043, Taiwan, ROC
[b] ITRI South, Industrial Technology Research Institute, Rm. 602, Bldg. 3, 31 Gongye 2nd Rd., Annan District, Tainan 70955, Taiwan, ROC
[c] Department of Chemical Engineering, National Taiwan University of Science and Technology, Taipei 10607, Taiwan, ROC
[d] Department of Chemical and Materials Engineering, National Chin-Yi University of Technology, Taichung 41101, Taiwan, ROC

ARTICLE INFO

Article history:
Received 3 August 2009
Received in revised form 6 October 2009
Accepted 9 October 2009
Available online 17 October 2009

Keywords:
Platinum oxide
Titanium dioxide
Visible light
Photocatalysis
Nitrogen oxides

ABSTRACT

The visible light active catalysts, PtO_x-doped TiO_2 (PtO_x–TiO_2) and PtO_x-loaded TiO_2 (PtO_x/TiO_2), were successfully synthesized by the acid-catalyzed sol–gel process and the impregnation method. $Pt(NH_3)_4(NO_3)_2$ or $H_2Pt(OH)_6$ was employed as the PtO_x precursor. By comparing the results of De-NO_x, the modified photocatalysts exhibited a higher visible-light-responsive activity, and a lower NO_2 selectivity than the unmodified ones. The FE-SEM images suggested that the particle size was unchanged after modification. The XRD patterns showed that the crystal structure still remained as anatase phase. Nitrogen adsorption revealed no significant change in surface areas for all samples. The UV–vis spectra indicated that PtO_x promoted the absorption of visible light. Furthermore, the XPS spectra evidenced that the mixed valence states of PtO–PtO_2 coexisted on the surface of TiO_2. The adding of PtO_x on TiO_2 not only promoted the visible-light-responsive activity of converting NO to NO_2 but also increased the consecutive reaction rate of NO_2 to NO_3^-.

1. Introduction

Since Fujishima and Honda's [1] discovery of the photo-induced water splitting on TiO_2 electrodes, photocatalysis based on powdered semiconductors has received much attention for the effective utilization of solar energy. Among all semiconductors, TiO_2 is the most widely studied photocatalyst, due to its strong redox ability, chemical stability, non-toxicity, and low cost. Recently, TiO_2 is extensively applied to environmental pollutant control, such as De-NO_x, De-VOCs, and water purification [2–6]. Unfortunately, the band gap of TiO_2 is 3.2 eV, corresponding to wavelengths of shorter than 388 nm. This fatal drawback limits the photocatalytic practice in the UV light region, which only counts for 4% of the solar spectrum, while the main part (45%) belongs to the visible light region. To overcome this shortcoming, many researchers have made much effort on the modification of TiO_2 to utilize sunlight more effectively and to further expand the indoor applications.

One approach to achieve the goal is non-metal doping. Sato [7] discovered the red-shift phenomena of a N-promoted TiO_2. Afterward, Asahi et al. [8] reported that a small amount of substitutional N atoms onto the TiO_2 structure by the sputtering method would induce the Ti^{3+} sites on the TiO_2 surface and significantly narrow the band gap. Nakamura et al. [9] found that TiO_2 treated with hydrogen plasma can generate oxygen vacancies and create sub-band gap to promote visible light responses, despite the expensive appliances. Organic dyes as the light sensitization agents were also considered to be added on the TiO_2 surface to improve the light efficiency [10,11]. However, the consumption of dye molecules during the reaction process obstructed the application.

Another approach is doping transitional metals into TiO_2 structure, such as Cr, V, Mn, Fe, Cu, or others [3,12–15]. However, the doping metal increases carrier-recombination rates on TiO_2 and reduces the thermal stability. Thus, metal-doped TiO_2 usually shows an increased visible light activity at the expense of UV activity. Recently, noble metals have been paid more attention as dopants for TiO_2 modification. Ohno et al. [16] demonstrated that the photo-oxidation of water takes place on the Ru-loaded TiO_2 powder under visible light. The stronger ability of electron capture by noble metals is postulated to extend the lifetime of the electron–hole pairs, hinder the recombination of them, and hence indirectly enhance the photocatalytic activity. Thus, the metallic Pt-loaded TiO_2 prepared by photodeposition has an improved UV activity in spite of no visible response [17,18]. However, Vorontsov

* Corresponding author at: Department of Chemical Engineering, National Tsing-Hua University, #101, Sec. 2, Kung-Fu Rd., Hsinchu 30043, Taiwan, ROC. Tel.: +886 3 5713763; fax: +886 3 5724725.
** Corresponding author. Tel.: +886 6 3847432; fax: +886 6 3847288.
E-mail addresses: ikwang@che.nthu.edu.tw (I.-K. Wang), YuMingLin@itri.org.tw (Y.-M. Lin).

1381-1169/$ – see front matter © 2009 Elsevier B.V. All rights reserved.
doi:10.1016/j.molcata.2009.10.015

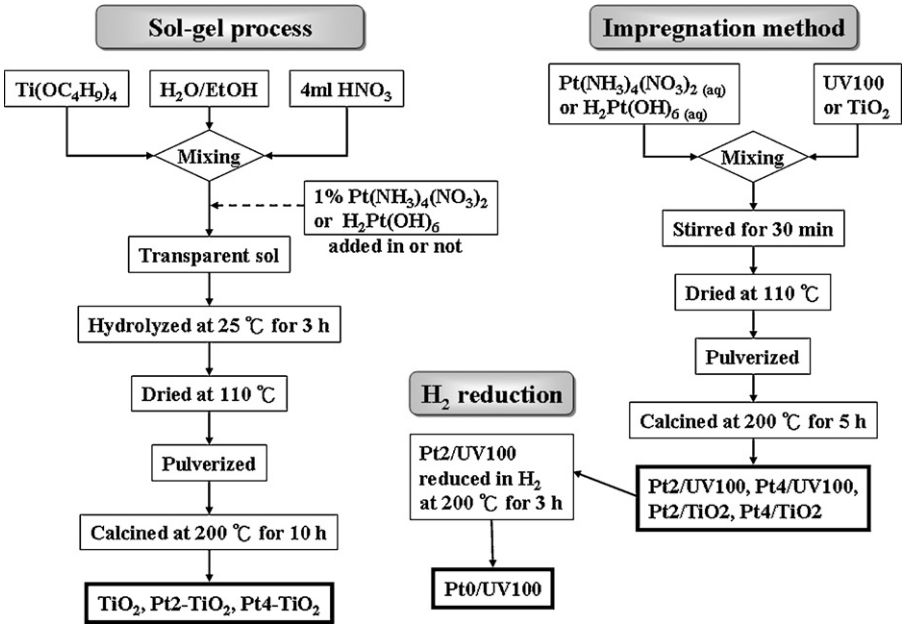

Fig. 1. Scheme of synthesis procedure.

et al. [19] reported that the photocatalytic activities depend on Pt states. Kisch and Macyk [20] have also found that the Pt complex doped TiO_2 promotes the visible activities. The oxidized state of Pt was confirmed to facilitate visible response and was more thermally stable during heat treatment process than metallic Pt.

Based on the economic consideration, our previous research [21] demonstrated that the visible-responsive photocatalyst, Pt/TiO_2, can be easily synthesized by sol–gel process or by impregnation method to load PtO_x on TiO_2. In this study, we planned to further improve the visible activities of photocatalysts and to investigate the relationship of the chemical states of PtO_x and the photoactivities.

2. Experimental

2.1. Preparation of photocatalysts

Two kinds of titania (TiO_2) were used as the raw materials for modification. One was commercially available TiO_2, Hombikat UV100 (Sachtleben Chemie, 100% anatase), and the other was synthesized by acid-catalyzed sol–gel process as described elsewhere [21]. Two types of platinum-containing compounds, tetra-amine platinum nitrate ($Pt(NH_3)_4(NO_3)_2$, symbolized by Pt2) and hydrogen hexa-hydroxy platinate ($H_2Pt(OH)_6$, symbolized by Pt4), were used to prepare 1% PtO_x/TiO_2.

For the purpose of doping Pt complex into the TiO_2 matrix, Pt2 or Pt4 with a desired atomic ratio of Pt/Ti = 1/100 was added during the acid-catalyzed sol–gel process. The synthesized photocatalysts were labeled as Pt2-TiO_2 and Pt4-TiO_2. On the other hand, impregnation method was employed to load PtO_x on the surface of TiO_2. TiO_2 powder (either UV100 or home made TiO_2) was added into a Pt2 or Pt4 solution with an atomic ratio of Pt/Ti = 1/100. After stirring for 1 h, all the samples were dried at 110 °C for 4 h and then calcined at 200 °C for 5 h. Four modified photocatalysts by the impregnation method were labeled as Pt2/UV100, Pt4/UV100, Pt2/TiO_2 and Pt4/TiO_2. In addition, the Pt2/UV100 was reduced in a hydrogen flow with a flow rate of 50 mL/min at 200 °C for 3 h, and the resulting catalyst was labeled as Pt0/UV100.

The above-mentioned procedures are depicted in Fig. 1. Samples were divided into two groups, the UV100 series (UV100, Pt2/UV100, Pt4/UV100 and Pt0/UV100) and the TiO_2 series (TiO_2, Pt2-TiO_2, Pt2/TiO_2, Pt4-TiO_2 and Pt4/TiO_2). The symbols of "-" and "/" represent the modification via the sol–gel method and the impregnation method.

2.2. Degradation of NO_x on photocatalyst

Photocatalytic degradation of nitrogen oxides (De-NO_x) was carried out by the setup consisting of a continuous flow reactor connected to the gas suppliers and the analytic system, as shown

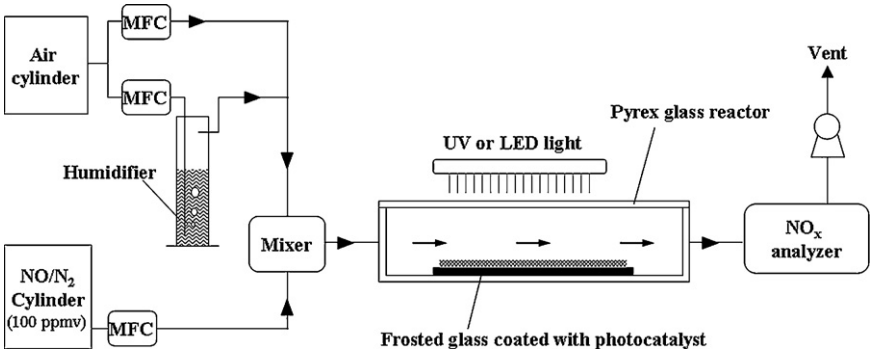

Fig. 2. Schematic diagram of De-NO_x system.

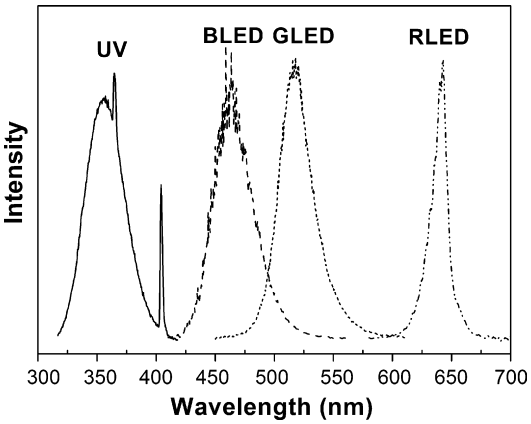

Fig. 3. Photon energy distribution of UV lamp and LEDs.

in Fig. 2. To simulate atmospheric environment and reach the optimal value, the relative humidity was fixed at 50% by adjusting a humidified air stream and a dry air stream [2]. Then, a nitric oxide (NO) gas stream, provided by a cylinder containing 100 ppmv NO (N_2 balance), was added to the air stream to reach a desired NO concentration of 1 ppmv and a total volumetric flow rate of 1 L/min. The photocatalyst (0.5 g) was added into an appropriate amount of D.I. water contained in a 50 mL flask, followed by well stirring. The mixed slurry was then slowly spread on a disk-like frosted glass (diameter = 12 cm). After drying at 110 °C for 30 min to remove water and remain sample powder on, the frosted glass coated with the photocatalyst was loaded into the reactor. A black light lamp over the reactor provided the ultraviolet illumination in the wavelength range of 330–420 nm. Light-emitting diodes (LEDs) provided the visible light illumination including blue LEDs (BLED, 430–530 nm), green LEDs (GLED, 470–570 nm), and red LEDs (RLED, 590–680 nm). The photon energy distribution profiles of the four irradiation sources are shown in Fig. 3. The intensity of the light was kept at 1 mW/cm^2, measured by a spectrophotometer (Ocean Optics, USB2000). Blank test was carried out under the same condition excluding the photocatalyst powder adding. The result ensured all the materials being inactive on photocatalytic De-NO_x.

Photocatalytic oxidation of NO on TiO_2 was investigated and a reaction pathway based on consecutive reactions with hydroxyl radicals, was proposed as follows [2]:

$$NO + OH^{\bullet} \rightleftharpoons HNO_2(H^+ + NO_2^-) \quad (1)$$

$$HNO_2 + OH^{\bullet} \rightleftharpoons NO_2 + H_2O \quad (2)$$

$$NO_2 + OH^{\bullet} \rightleftharpoons HNO_3(H^+ + NO_3^-) \quad (3)$$

In which, HNO_2 is a minor species and can be reversed to NO or oxidized to NO_2. Consequently, NO oxidation can be simplified in a serial mechanism of $NO \rightarrow NO_2 \rightarrow NO_3^-$ over photocatalyst under illumination. The effluent concentrations of NO and NO_2 from the reactor were measured by a NO_x analyzer (Eco Physics, CLD 700AL). The NO_3^- ion was adsorbed on the photocatalyst surface, and could be washed out by water. In data analysis, the total NO_x concentration ($[NO_x]$), the NO conversion, the NO_2 selectivity, and the total NO_x removal are defined as follows:

$$[NO_x] = [NO] + [NO_2] \quad (4)$$

$$\text{NO conversion} = \frac{[NO]_{in} - [NO]_{out}}{[NO]_{in}} \quad (5)$$

$$\text{NO}_2 \text{ selectivity} = \frac{[NO_2]_{out}}{[NO]_{in} - [NO]_{out}} \quad (6)$$

$$\text{total NO}_x \text{ removal} = \frac{[NO]_{in} - [NO_x]_{out}}{[NO]_{in}} \quad (7)$$

Since NO_2 is more toxic than NO [22,23], the photocatalyst performance should be evaluated by the total NO_x removal, or the NO conversion conjunctive with the NO_2 selectivity.

2.3. Characterization and analysis

The particle sizes and the morphology of the synthesized samples were determined by a field-emission scanning electron microscopy (FE-SEM, Hitachi S4800-1).

The crystal structures were analyzed by an X-ray powder diffractometry (XRD, Rigaku RU-H3R) in the reflection mode with Cu K_α radiation. The angular domain was 20–80° (2θ). In addition, the grain sizes (d) were calculated by Scherrer's equation, as follows:

$$d = \frac{0.9\lambda}{\beta \cos\theta} \quad (8)$$

where λ is the X-ray source wavelength of 1.5405 Å and β is the full width at half maximum of main peak.

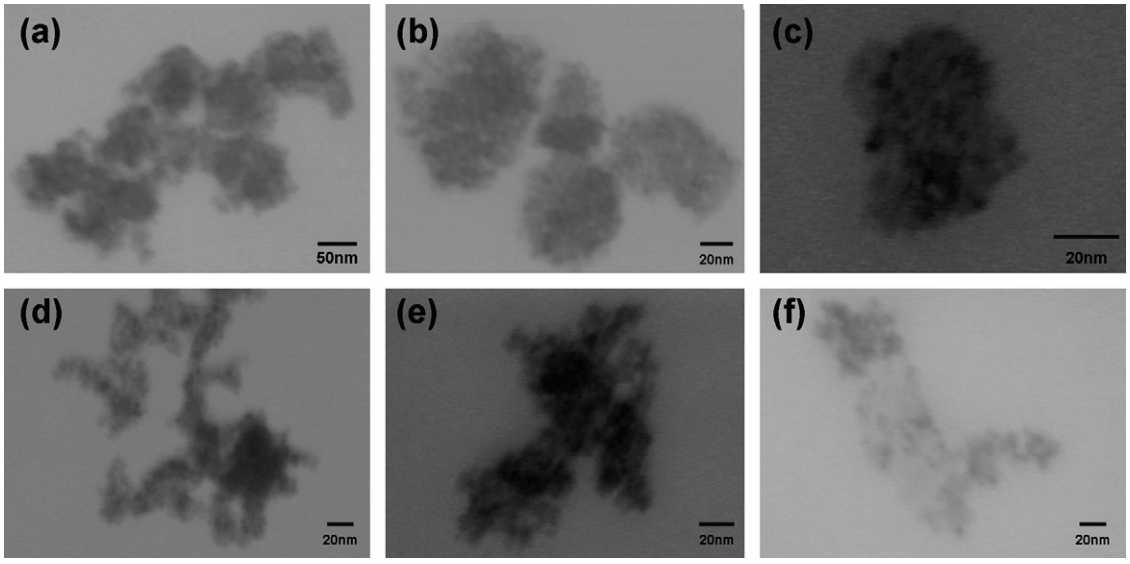

Fig. 4. FE-SEM images of the photocatalysts with (a) UV100, (b) Pt2/UV100, (c) Pt4/UV100, (d) TiO_2, (e) Pt2-TiO_2, and (f) Pt2/TiO_2.

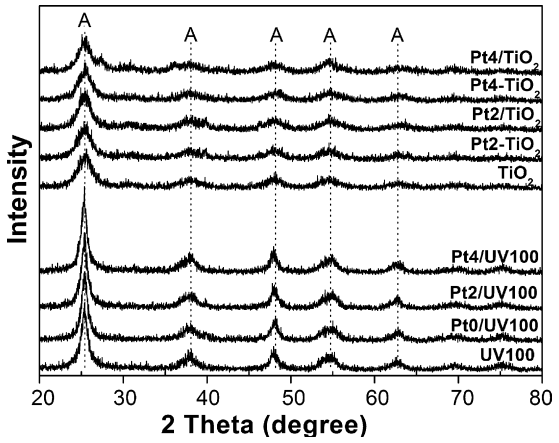

Fig. 5. XRD patterns of the photocatalysts.

The specific surface areas were measured by nitrogen adsorption at 77 K using a Micrometrics model ASAP 2000 instrument. All the samples were outgassed to a vacuum of $<10^{-4}$ Torr at 200 °C for 2 h to remove any adsorbed impurities prior to each measurement. Surface areas were calculated by BET method.

The UV–vis absorption spectra of all samples were measured by a powder UV–vis spectrophotometer (UV-VIS, Shimadzu UV-2450). The obtained reflectance data (R) were converted to the absorbance values, $F(R)$, based on the Kubelka–Munk theory, as follows:

$$F(R) = \frac{(1-R)^2}{2R} \quad (9)$$

The surface atomic composition of the catalysts and the chemical states of Pt were examined by an X-ray photoelectron spectroscopy (XPS, Physical Electronics ESCA PHI 1600) with Mg K_α radiation. The charging effects were corrected by adjusting the C 1s peak to a position of 284.5 eV.

3. Results and discussion

3.1. Characterization

3.1.1. Morphology

Fig. 4 shows the FE-SEM images of various photocatalysts. The particle sizes of UV100 series (UV100, Pt2/UV100 and Pt4/UV100) were similar, around 7–12 nm. It suggested that the primary particle sizes were unchanged after impregnating PtO_x. The particle sizes of TiO_2 series (TiO_2, Pt2-TiO_2 and Pt2/TiO_2) were smaller (around 3–10 nm) and more dispersive, except for Pt2-TiO_2, which implied the morphology tended to be more agglomerative by sol–gel method than that by impregnation method. This could be rationalized that the platinic precursor was added during hydrolysis of titanium alkoxide prior to crystalline phase formation. On the other hand, the impregnation method, platinic precursor was loaded on the well-formed crystalline TiO_2 particles.

Table 1
The surface areas, atomic compositions and calculated atomic ratios for all samples.[a].

Samples	S_{BET} (m^2/g)	Atomic composition (%)					Atomic ratio	
		Ti	O	C	N	Pt	O/Ti	Pt/Ti
UV100	249	15.7	58.9	24.0	1.4	–	3.75	–
Pt0/UV100	250	16.3	55.9	25.6	2.0	0.2	3.42	0.01
Pt2/UV100	260	17.0	57.8	22.4	2.6	0.2	3.40	0.01
Pt4/UV100	272	17.1	54.6	26.5	1.5	0.3	3.19	0.02
TiO_2	254	12.9	54.7	31.0	1.4	–	4.24	–
Pt2-TiO_2	244	15.0	52.3	31.0	1.4	0.3	3.49	0.02
Pt2/TiO_2	256	16.3	52.6	29.9	0.9	0.3	3.23	0.02
Pt4-TiO_2	226	17.0	49.1	33.5	0.2	0.2	2.89	0.01
Pt4/TiO_2	217	20.2	47.1	31.9	0.4	0.4	2.33	0.02

[a] All samples were calcined at 200 °C.

3.1.2. Crystal structure

The XRD patterns are shown in Fig. 5. All the crystal structures of samples were almost anatase, attributed to several main peaks ($2\theta = 25.3°$ with [1 0 1], 37.8° with [0 0 4], 48.1° with [2 0 0], 54.0° with [1 0 5], 62.7° with [2 0 4]). Since all samples were calcined at a relatively low temperature of 200 °C and only a small amount of PtO_x (1%) was added in, there was no significant difference among the samples. The PtO_x was interpreted as well-dispersed by the evidence of the absence of Pt signal.

According to Scherrer's equation by introducing the full width at half maximum of main peak with $2\theta = 25.3°$ for anatase phase, the grain size is larger with the sharper main peak. The calculated result revealed that the grain size of UV100 series was around 9–12 nm, and that of TiO_2 series around 5–6 nm. The results were consistent with the FE-SEM images. Besides, the FE-SEM results also suggested that there is no significant change in particle size before and after PtO_x loading.

3.1.3. Surface area

The surface areas of all samples, around 217–272 m^2/g, are listed in Table 1. For UV100 series, the three modified samples of Pt0/UV100, Pt2/UV100 and Pt4/UV100 showed no significant change or only a slight increase with 250, 260 and 272 m^2/g, respec-

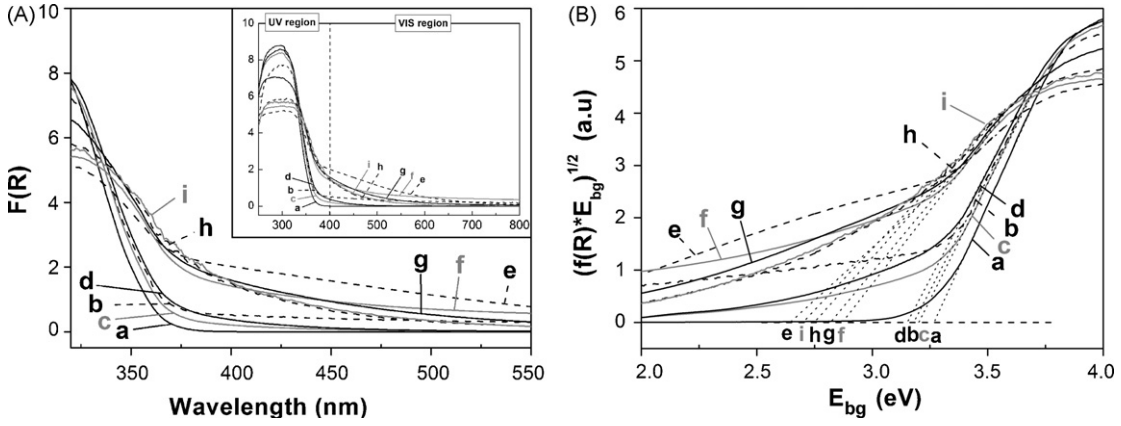

Fig. 6. (A) UV–vis absorption spectra and (B) plot of transformed Kubelka–Munk function versus the energy of the light absorbed for (a) UV100, (b) Pt0/UV100, (c) Pt2/UV100, (d) Pt4/UV100, (e) TiO_2, (f) Pt2-TiO_2, (g)Pt2/TiO_2, (h)Pt4-TiO_2, and (i)Pt4/TiO_2, with the direct band gap of (a) 3.26, (b) 3.18, (c) 3.20, (d) 3.15, (e) 2.65, (f) 2.87, (g) 2.82, (h) 2.75, and (i) 2.70 eV.

tively, compared to the sample of UV100 (249 m^2/g). This was reasonable that the small amount metallic Pt or PtO_x could be well-dispersive on crystalline TiO_2 powder by impregnation method. The home made TiO_2 possessed the surface area of 254 m^2/g, similar to UV100. This result was also corresponding to their similar particle sizes. After modification, the four samples of Pt2-TiO_2, Pt2/TiO_2, Pt4-TiO_2 and Pt4/TiO_2 showed unchanged or some decrease in surface areas with 244, 256, 226 and 217 m^2/g, respectively.

3.1.4. UV–vis absorption

The UV–vis absorbance spectra are presented in Fig. 6A, used to determine the light absorption initially. For UV100 series ((a)–(d)), UV100 displayed no visible absorption due to its single and wide band gap. After the treatment of loading metallic Pt or PtO_x, each of Pt0/UV100, Pt2/UV100 and Pt4/UV100 exhibited small raise of the visible absorption. On the other hand, the home made TiO_2 had evident absorption in the visible light region, which was attributed to the carbonaceous residues during sol–gel process [24]. After PtO_x modification either by sol–gel process or by impregnation method, the four PtO_x-modified TiO_2 (Pt2-TiO_2, Pt2/TiO_2, Pt4-TiO_2 and Pt4/TiO_2) showed decrease in visible absorption band. It is possible that some carbonaceous species in the PtO_x-modified TiO_2 samples were decomposed again during secondary calcination. Despite of that, all the modified samples and the home made TiO_2 showed significant visible light absorbance.

For semiconductor materials, the direct band gap can be obtained by constructing Tauc Plot—$(F(R) \times h\nu)^{1/2}$ versus $h\nu$ [25]. As shown in Fig. 6B, the interception (represented by the dotted lines), which is the extension of the linear region until the base line, gives the so-called Tauc optical band gap. It was obtained that the band gap of UV100 (3.26 eV) was corresponding to the wavelengths shorter than 380 nm with only UV light absorbance. The modified samples of Pt0/UV100, Pt2/UV100 and Pt4/UV100 showed some red shift to 3.18, 3.20 and 3.15 eV, respectively. The red shift qualitatively qualified the catalyst to be activated under visible light illumination. For the TiO_2 series, unmodified TiO_2 had the relatively lowest band gap of 2.65 eV. PtO_x-modified TiO_2 showed a slight blue shift, but still located in the visible light region. To summarize, the direct band gaps of all samples were in the order of TiO_2 < Pt4/TiO_2 < Pt4-TiO_2 < Pt2/TiO_2 < Pt2-TiO_2 < Pt4/UV100 < Pt0/UV100 < Pt2/UV100 < UV100.

3.2. XPS analysis of chemical elements and electronic structure

3.2.1. Atomic composition

XPS analysis revealed the surface constitution of the samples. The atomic compositions and calculated atomic ratios of O/Ti and Pt/Ti for all samples are listed in Table 1. The carbon content was unexpectedly high, about 24–33.5%. It was confirmed that the most carbon arose from adventitious element carbon corresponding to the peak at 284.5 eV [26]. Noteworthily, the carbon percentages of TiO_2 series were all higher than those of UV100 series. The existence of carbonaceous species of home made TiO_2 might be derived from alkyl groups during sol–gel process and were not completely removed out at a calcining temperature of 200 °C.

The small amount of nitrogen might come from the residual impurity of UV100, the nitric acid for sol–gel process, and the Pt2 precursor ($Pt(NH_3)_4(NO_3)_2$) for modification. As the data revealed, the samples modified by Pt4 had lower nitrogen amounts than those modified by Pt2. Moreover, samples using home made TiO_2 as raw materials also showed less nitrogen than those using UV100. The atomic ratios of O to Ti for all samples were higher than 2, attributed by the hydrophilic property of TiO_2, causing H_2O molecules to be chemisorbed on. It was also found that all the O/Ti values of the modified samples were lower than those of the bare titania. The decreasing hydrophilic property was referred to the existence of PtO_x on the surface.

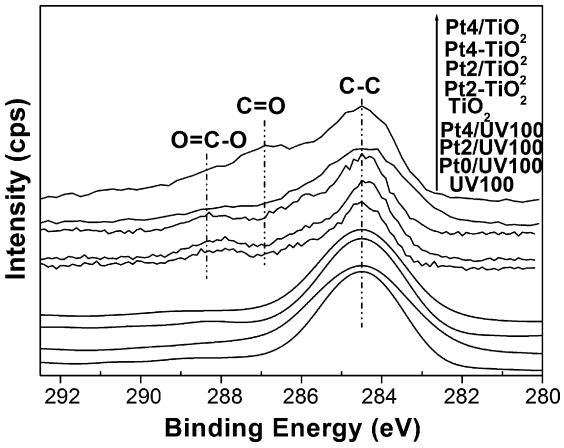

Fig. 7. C 1s XPS spectra of all samples.

The ratios of Pt to Ti were higher than or equal to the anticipated ratio (1%). It was due to the surface sensitive property of XPS. The result also implied that most PtO_x tended to be on the titania surface rather than in structure, whether synthesized by sol–gel or impregnation method.

3.2.2. Analysis of chemical states

The chemical states of elements in materials could be provided by XPS spectra. The Ti 2p XPS spectra of all samples represented insignificant variation (almost Ti^{4+} signal), and the Ti^{3+} signal was not found. The C 1s XPS spectra of all samples are demonstrated in Fig. 7. It can be seen that UV100 series had only one carbon state with the peak located at 284.5 eV corresponding to adventitious carbon, while TiO_2 series had two more shoulder peaks located at 287 and 288.5 eV, corresponding to C=O and O=C–O, respectively. Sakthivel and Kisch [27] reported that the two kinds of carbonate species could be observed via hydrolysis process followed by calcinations. Li et al. [28] also mentioned that the carbon, in the form of carbonate instead of substituting form, may narrow the band gap and induce visible response to oxidation of gaseous benzene. This also provides an explanation why the visible light absorbance of TiO_2 series was higher than that of UV100 series. And it could be anticipated that home made TiO_2 would exhibit more visible activity than UV100 due to the carbonate residues.

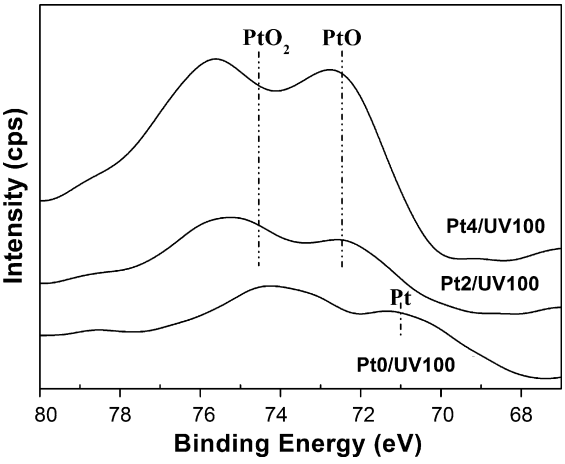

Fig. 8. Pt 4f XPS spectra of various Pt loaded onto UV100.

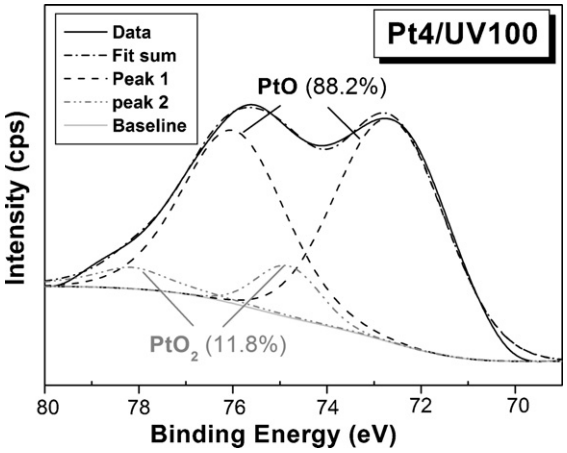

Fig. 9. The deconvolution of Pt 4f XPS spectra for Pt4/UV100.

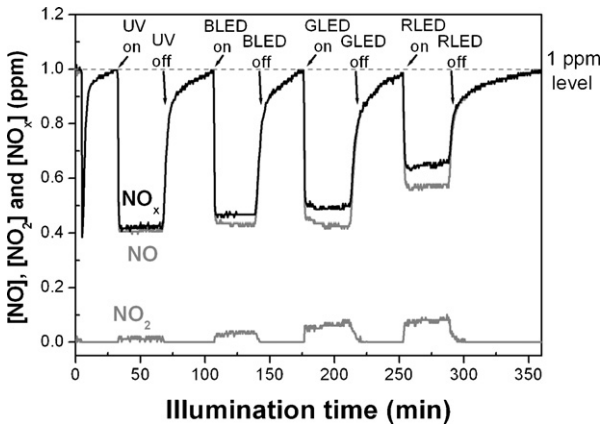

Fig. 10. Time dependency profile of NO, NO_2 and NO_x concentrations as a function of illumination time on Pt4/TiO_2 under UV, BLED, GLED and RLED illumination: catalyst loading, 0.5 g; irradiation intensity, 1 mW/cm^2; feed concentration of NO, 1 ppmv; inlet flow rate, 1 L/min; relative humidity, 50%; and reaction temperature, 25 °C.

The Pt 4f XPS spectra of Pt0/UV100, Pt2/UV100 and Pt4/UV100 are shown in Fig. 8. The binding energy at 71.2 eV indicated the reduced state of Pt^0 of Pt0/UV100. The nearly single Pt^0 state was only found on Pt0/UV100, attributed to the treatment of hydrogen reduction. For a single oxide valence state of Pt, the integral intensity ratio of $4f_{7/2}$ to $4f_{5/2}$ should be 4:3 in theory. However, our results showed mixed valence states of Pt on Pt2/UV100 and Pt4/UV100 evidenced by the discordant ratio of integral intensity. To determine them, peak deconvolution was employed by using the binding energy of $4f_{7/2}$ for Pt^0, Pt^{2+} and Pt^{4+} as 71.2, 72.5 and 74.8 eV, respectively. The deconvolution of Pt 4f XPS spectra for Pt4/UV100 is presented as a representative example in Fig. 9, and the results for the three samples are listed in Table 2. Pt0/UV100 contained mainly Pt^0 (94.4%) and some Pt^{2+} (5.6%), indicating a mainly metallic state. The Pt states of Pt2/UV100 were similar to those of Pt4/UV100, major Pt^{2+} and minor Pt^{4+}. It inferred that PtO_x was in the form of coexistent PtO–PtO_2 on the TiO_2 surface, either using Pt^{2+} (from $Pt(NH_3)_4(NO_3)_2$) or Pt^{4+} (from $H_2Pt(OH)_6$) ion as the precursor. It was reasonable as both of them were calcined at the same temperature. Kisch and Macyk [20] reported the behavior of TiO_2 modified with $PtCl_4$ in the bulk or on the surface. The excited platinum complex underwent bond cleavage to afford electron transfer to TiO_2 and resulted in the shift of flatband potential. It also increases the driving force of electron transfer from Pt^{3+} intermediate and therefore improves the activity [20]. Consequently, the mixed valence states of PtO_x at the surface of TiO_2 were regarded as a sensitizer responding to the visible light.

The N 1s XPS spectra of Pt2/UV100, not shown here, presented two types of peaks. The major peak located at 400.5 eV was considered as nitrogen impurity originated from the bulk, and the minor peak located at 407.4 eV was considered as nitrates attributed to the Pt2 precursor ($Pt2(NH_3)_4(NO_3)_2$). It was reasonable that nitrates could not be totally removed out after low temperature calcination. Some research groups reported that the peak at 396 eV, derived from the substitutional N (β-N), was considered as the visible light source [8]. However, β-N peak was not found in our all samples.

Table 2
The results of deconvolution from various Pt loaded onto UV100.

(%)	Pt $4f_{7/2}$		
	Pt^0% (71.2 eV)	Pt^{2+} % (72.5 eV)	Pt^{4+} % (74.8 eV)
Pt0/UV100	94.4	5.6	–
Pt2/UV100	–	82.7	17.3
Pt4/UV100	–	88.2	11.8

This also implied that the residual species from $Pt(NH_3)_4(NO_3)_2$ did not form the substitutional N in the TiO_2 structure as expected and could not further cause visible light response.

3.3. Photocatalytic activity

To illustrate the behavior of photocatalytic De-NO_x, 0.5 g powder photocatalyst was used under 1 mW/cm^2 intensity of various light illumination (UV, BLED, GLED and RLED). The typical time dependency profile of NO, NO_2 and NO_x concentrations is shown in Fig. 10. NO with a concentration of 1 ppmv was introduced into the reactor under dark condition. After a few minutes, as the adsorption was reached to equilibrium, the light was turned on. The durability of the catalyst was confirmed by repeating above procedures with different light source as shown in Fig. 10.

It was reported that the oxidation reaction can only go as far as NO_2 once the catalyst is saturated with NO_3^- [2]. Ohko et al. [29] studied the reaction of NO on a HNO_3 pre-deposited TiO_2 under UV light illumination and proposed a side reaction of $NO + NO_3 \rightarrow 2NO_2$. However, this side reaction may only occur as the support was saturated with NO_3^-. This phenomenon was not found in our case due to the NO_2 concentration approximately maintained a stable value, and the large surface area of the catalyst (217–272 m^2/g) was unable to be saturated with NO_3^- during a few hours operation.

By Eqs. (5)–(7), the NO conversion (NOC), NO_2 selectivity (NO_2S) and total NO_x removal (NO_xR) over various photocatalysts are shown in Figs. 11 and 12. The NO conversion represents the oxidation percentage of NO to NO_2 and NO_3^-. The total NO_x removal expresses the total reaction percentage of producing NO_3^-, considered as the total oxidation ability. A well-active photocatalyst should basically provide a high NO conversion as well as a low NO_2 selectivity, resulting in a high total NO_x removal. In other words, with the same NO conversion, the one with lower NO_2 selectivity could catalyze the oxidation of NO_2 to NO_3^- more completely.

The performances of the two bare TiO_2 (UV100 (Fig. 11A) and home made TiO_2 (Fig. 12A)) were compared with each other under UV light illumination. Although UV100 exhibited a higher NO conversion (UV100 = 71%; TiO_2 = 61%), the total NO_x removal was less than home made TiO_2 (UV100 = 51%; TiO_2 = 57%) due to the variations in NO_2 selectivity. It implied the latter one had better ability of total oxidation. For visible light activity, the home made TiO_2 showed not only a higher NO conversion but also a higher total NO_x removal than UV100, especially in GLED and RLED. The better visible activity of home made TiO_2 was attributed to the carbonate

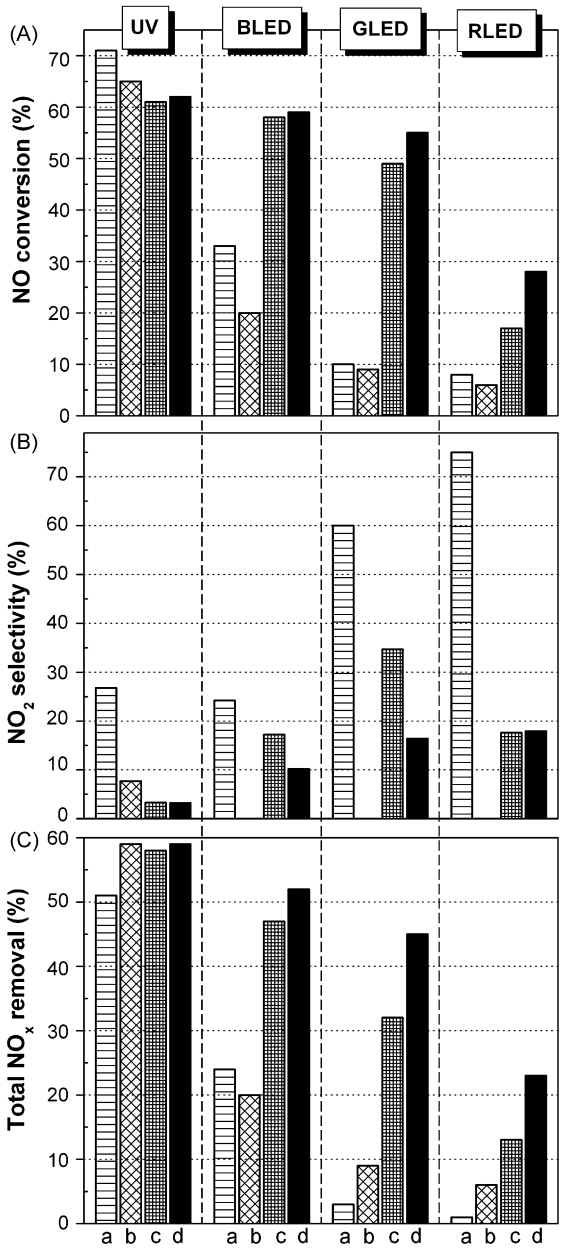

Fig. 11. De-NO_x activities on UV100 series consisting of (A) NO conversion, (B) NO_2 selectivity and (C) total NO_x removal for (a) UV100, (b) Pt0/UV100, (c) Pt2/UV100 and (d) Pt4/UV100 under different light illumination.

species residual from the alkyl oxide precursor and alcohol in the sol–gel process, as evidenced in XPS result.

Fig. 11 gives the results of De-NO_x over various photocatalysts with UV100 as the modifiable material. Pt0/UV100 (b), with metallic Pt^0 state, exhibited a higher UV total NO_x removal than UV100, but no significant improvement under visible light illumination. However, the low NO_2 selectivity confirmed that Pt0/UV100 improved the total oxidation of NO to NO_3^-. Vorontsov et al. [19] also reported that the photocatalytic activity of Pt/TiO_2 depends on the Pt states. Deconvolution of the XPS spectrum for Pt0/UV100 showed of the occurrence of mainly Pt^0 state. The reduced state of Pt functioned not only as the electron trap center but also as the adsorption center of O_2 to facilitate the total oxidation [30,31]. However, Pt^0 state was helpless to visible light activity. On the other hand, evident improvement of visible light activity on both Pt2/UV100 and Pt4/UV100 (c and d) was observed. Additionally, NO_2 selectivity was also abated by the two samples compared to bare UV100, even though the lowest NO_2 selectivity was found on Pt0/UV100. Overall, the result proved that PtO–PtO_2 loaded TiO_2 not only exhibited the ability of NO_2 abatement, but also provided sufficient visible light activity. Pt2/UV100 and Pt4/UV100 possessed the similar Pt states (PtO–PtO_2), but the former was less active under visible light, caused by the different Pt precursors. XPS spectra revealed that no any β-N peak was found. In other words, the residual nitrates from $Pt(NH_3)_4(NO_3)_2$ precursor could not be totally removed out and did not form the substitutional N in the TiO_2 structure as expected after low temperature calcination. Therefore, the nitrates were helpless to visible light activity and just acted as impurities. Compared to this, $H_2Pt(OH)_6$ was used as the Pt precursor to prepare Pt4/UV100 and subsequently formed PtO–PtO_x on TiO_2 surface without any other impurities. It may be the reason why Pt4/UV100 showed the best De-NO_x activity among UV100 series whether under UV or visible illumination.

When using the home made TiO_2 as raw material, as shown in Fig. 12, the four modified samples (Pt2-TiO_2 (b), Pt4-TiO_2 (c),

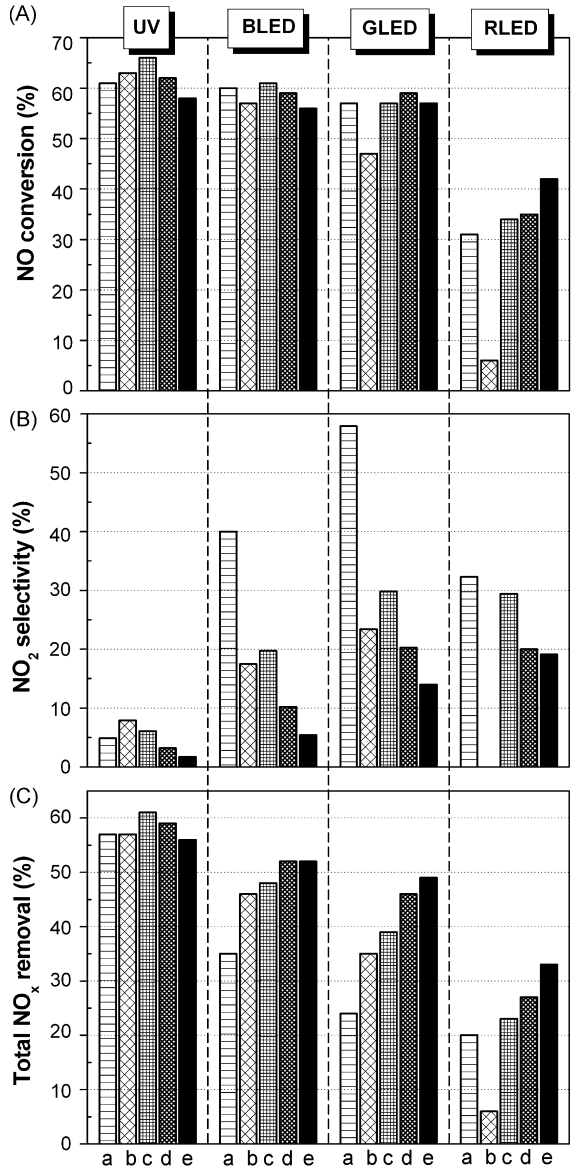

Fig. 12. De-NO_x activities on TiO_2 series consisting of (A) NO conversion, (B) NO_2 selectivity and (C) total NO_x removal for (a) TiO_2, (b) Pt2-TiO_2, (c) Pt4-TiO_2, (d) $Pt2/TiO_2$ and (e) $Pt4/TiO_2$ under different light illumination.

Pt2/TiO_2 (d) and Pt4/TiO_2 (e)) offered around the same UV activity as the bare TiO_2 (a). Under the illumination of visible light, four modified samples seemed not to present noticeably higher NO conversion than bare TiO_2. It was reasonable that the home made TiO_2 performed well visible light activity resulted from the carbonate species residual, as described in XPS result. However, the four modified samples, except for Pt2-TiO_2 under RLED, performed higher total NO_x removal under visible light illumination, due to the decrease of NO_2 selectivity. The results confirmed again that the existence of PtO_x would promote the total oxidation of NO to NO_3^-. For Pt2-TiO_2, even in the presence of PtO_x, hydrolysis process may cause the PtO_x and unnecessary nitrate residues to be doped in TiO_2 matrix, and therefore reduce the visible efficiency.

In addition, Pt2/TiO_2 and Pt4/TiO_2 showed more activity than Pt2-TiO_2 and Pt4-TiO_2 in visible region, suggesting that PtO_x on the TiO_2 surface was more beneficial for visible response than in the matrix. On the other hand, by using either UV100 or home made TiO_2 as the raw material, the relative conversion increased in the order of unmodified one < Pt2 < Pt4. It suggested the platinic precursor of $H_2Pt(OH)_6$ was more useful than $Pt(NH_3)_4(NO_3)_2$, because of the latter would arise some nitrate impurities. It could be conclude that the visible sensitizer of mixed PtO–PtO_2 would function better on TiO_2 surface via impregnation method than in TiO_2 matrix via sol–gel method. And using $H_2Pt(OH)_6$ as the precursor was beneficial to form PtO–PtO_2 without other impurities.

To summarize, for UV100 series, photocatalytic activities were in the order of UV100 < Pt2/UV100 < Pt4/UV100. For TiO_2 series, they were in the order of TiO_2 < Pt2-TiO_2 < Pt4-TiO_2 < Pt2/TiO_2 < Pt4/TiO_2. The Pt4/TiO_2, prepared by the sol–gel process and followed by impregnation with $H_2Pt(OH)_6$ as a PtO_x dopant, exhibited the highest visible activity among all. Even under red light illumination, the total NO_x removal could reach a level of 33%. The visible sensitizer of PtO_x loaded on the TiO_2 surface was better than that doped in TiO_2. Moreover, the particle size, surface area and the crystal structure remained roughly unchanged with adding only 1% PtO_x.

4. Conclusions

In this study, the Pt4/TiO_2 photocatalyst, which was synthesized by sol–gel process followed by impregnation with $H_2Pt(OH)_6$, exhibited a notable visible activity for NO_x degradation, compared to bare TiO_2. The results of characterization revealed that the particle size, the crystal structure and the surface area were unchanged after modification with 1% PtO_x and undergoing 200 °C calcination. The chemical state of platinum species played an important role in photocatalysis. It was evidenced that the mixed valence states of PtO–PtO_2 coexisted on the surface of TiO_2. The PtO–PtO_2 was regarded not only as a sensitizer responding to the visible light but also to facilitate the oxidation of NO_2 to NO_3^- by suppression the NO_2 selectivity.

References

[1] A. Fujishima, K. Honda, Nature 238 (1972) 37.
[2] S. Devahasdin, C. Fan Jr., K. Li, D.H. Chen, J. Photochem. Photobiol. A: Chem. 156 (2003) 161.
[3] M.R. Hoffmann, S.T. Martin, W. Choi, D.W. Bahnemannt, Chem. Rev. 95 (1995) 69.
[4] A. Fujishima, T.N. Rao, D.A. Tryk, J. Photochem. Photobiol. C: Photochem. Rev. 1 (2000) 1.
[5] J.C.S. Wu, Y.T. Cheng, J. Catal. 237 (2006) 393.
[6] Y. Ohko, Y. Nakamura, A. Fukuda, S. Matsuzawa, K. Takeuchi, J. Phys. Chem. C 112 (2008) 10502.
[7] S. Sato, Chem. Phys. Lett. 123 (1986) 126.
[8] R. Asahi, T. Morikawa, T. Ohwaki, K. Aoki, Y. Taga, Science 293 (2001) 269.
[9] I. Nakamura, N. Negishi, S. Kutsuna, T. Ihara, S. Sugihara, K. Takeuchi, J. Mol. Catal. A: Chem. 161 (2000) 205.
[10] C. Nasr, K. Vinodgopal, L. Fisher, S. Hotchandani, A.K. Chattopadhyay, P.V. Kamat, J. Phys. Chem. 100 (1996) 8436.
[11] T. Wu, G. Liu, J. Zhao, H. Hidaka, N. Serpone, J. Phys. Chem. B 103 (1999) 4862.
[12] M. Anpo, M. Takeuchi, K. Ikeue, S. Dohshi, Curr. Opin. Solid State Mater. Sci. 6 (2002) 381.
[13] H. Yamashita, M. Harada, J. Misaka, M. Takeuchi, K. Ikeue, M. Anpo, J. Photochem. Photobiol. A: Chem. 148 (2002) 257.
[14] S. Klosek, D. Raftery, J. Phys. Chem. B 105 (2001) 2815.
[15] Y. Sakata, T. Yamamoto, T. Okazaki, H. Imamura, S. Tsuchiya, Chem. Lett. 27 (1998) 1253.
[16] T. Ohno, F. Tanigawa, K. Fujihara, S. Izumi, M. Matsumura, J. Photochem. Photobiol. A: Chem. 127 (1999) 107.
[17] K.C. Cho, K.C. Hwang, T. Sano, J. Photochem. Photobiol. A: Chem. 161 (2004) 155.
[18] S.H. Chien, M.C. Kuo, C.H. Lu, Catal. Today 97 (2004) 121.
[19] A.V. Vorontsov, E.N. Savinov, J. Zhensheng, J. Photochem. Photobiol. A: Chem. 125 (1999) 113.
[20] H. Kisch, W. Macyk, ChemPhysChem 3 (2002) 399.
[21] Y.M. Lin, Y.H. Tseng, J.H. Huang, C.C. Chao, C.C. Chen, I.K. Wang, Environ. Sci. Technol. 40 (2006) 1616.
[22] O.I. Miller, D.S. Celermajer, J.E. Deanfield, D.J. Macrae, Arch. Dis. Child 70 (1994) 47.
[23] R.S. Wade, C.E. Castro, Chem. Res. Toxicol. 9 (1996) 1382.
[24] C. Lettmann, K. Hildenbrand, H. Kisch, W. Macyk, W.F. Maier, Appl. Catal. B: Environ. 32 (2001) 215.
[25] Tauc, R. Grigorovici, A. Vancu, Phys. Stat. Sol. 15 (1966) 627.
[26] E. Papirer, R. Lacroix, J.B. Donnet, G. Nanse, P. Fioux, Carbon 33 (1995) 63.
[27] S. Sakthivel, H. Kisch, Angew. Chem. Int. Ed. 42 (2003) 4908.
[28] Y. Li, D.S. Hwang, N.H. Lee, S.J. Kim, Chem. Phys. Lett. 404 (2005) 25.
[29] Y. Ohko, Y. Nakamura, N. Negishi, S. Matsuzawa, K. Takeuchi, J. Photochem. Photobiol. A: Chem. 205 (2009) 28.
[30] J. Yang, D. Li, Z. Zhang, Q. Li, H. Wang, J. Photochem. Photobiol. A: Chem. 137 (2000) 197.
[31] A. Sclafani, J.M. Herrmann, J. Photochem. Photobiol. A: Chem. 113 (1998) 181.